RAA 2021 Vol. **21** No. **5**, 129(9pp) doi: 10.1088/1674-4527/21/5/129

http://www.raa-journal.org *http://iopscience.iop.org/raa*

***R**esearch in*
***A**stronomy and*
***A**strophysics*

Heavy element contributions of rotating massive stars to interstellar medium

Rui-Qing Wu, Chun-Hua Zhu, Guo-Liang Lü, Zhao-Jun Wang and He-Lei Liu

School of Physical Science and Technology, Xinjiang University, Urumqi 830046, China; *ruiqingwu163@163.com*, *chunhuazhu@sina.cn*

Received 2020 December 9; accepted 2021 January 12

Abstract Employing the stellar evolution code Modules for Experiments in Stellar Astrophysics (MESA), we calculate yields of heavy elements from massive stars via stellar wind and core−collapse supernova (CCSN) ejecta to the interstellar medium (ISM). In our models, the initial masses ($M_{\rm ini}$) of massive stars are taken from 13 to 80 $M_{\odot}$, their initial rotational velocities (V) are 0, 300 and 500 km s^{-1}, and their metallicities are $[{\rm Fe/H}] = -3, -2, -1$ and 0. The yields of heavy elements coming from stellar winds are mainly affected by stellar rotation which changes the chemical abundances of stellar surfaces via chemically homogeneous evolution, and enhances mass-loss rate. We estimate that the stellar wind can produce heavy element yields of about 10^{-2} (for low metallicity models) to a mass of several $M_{\odot}$ (for low metallicity and rapid rotation models). The yields of heavy elements produced by CCSN ejecta also depend on the large amount of remnant mass which is mainly determined by the mass of the CO-core. Our models calculate that the yields of heavy elements produced by CCSN ejecta can get up to several $M_{\odot}$. Compared with stellar wind, CCSN ejecta has a greater contribution to the heavy elements in ISM. We also compare the ^{56}Ni yields calculated in this work with the observational estimate. Our models only explain the ^{56}Ni masses produced by faint SNe or normal SNe with progenitor mass lower than about 25 $M_{\odot}$, and greatly underestimate the ^{56}Ni masses produced by stars with masses higher than about 30 $M_{\odot}$.

Key words: Stars: massive — rotation — ISM: abundances

1 INTRODUCTION

The interstellar medium (ISM) has the following constituents: atomic, gas ions, dust grains, cosmic rays and also many molecules. Heavy elements are fundamental components in the ISM and play a critical role in the stellar evolution of astrophysics and chemical evolution in the ISM. It is well known that massive stars with an initial mass larger than $\sim 8\,M_{\odot}$ play the most important role in producing heavy elements in the ISM (e.g., Dunne et al. 2003; Ablimit & Maeda 2018; Du 2020). These massive stars contribute to heavy elements via stellar wind and the ejecta of core−collapse supernovae (CCSNe). Although the heavy elements may originate from other sources including the stellar wind of asymptotic giant branch stars, ejecta of classical novae, binary merger, etc., their contribution is very low (Groenewegen & de Jong 1993; Marigo 2007; Hix 2001; Lü et al. 2013; Zhu et al. 2013; José et al. 2006; Li et al. 2016; Rukeya et al. 2017; Zhu et al. 2019; Duolikun et al. 2019; Shi et al. 2020; Guo et al. 2020).

The yields of heavy elements from massive stars have been investigated by many literatures (e.g., Woosley & Weaver 1995; Chieffi & Limongi 2004; Nomoto et al. 2006; Heger & Woosley 2010; Nomoto et al. 2013). However, these works do not consider mass loss which is very important for massive star evolution (A recent review can be seen in Smith 2014). Usually, the mass loss was thought to be caused by stellar wind driven by strong radiation (Castor et al. 1975; Puls et al. 2008). Simultaneously, it is also affected by metallicity and rotation (Vink 2000; Vink et al. 2001; Meynet 2000; Maeder & Meynet 2012). Because the efficiency of radiation pressure in removing the stellar envelope depends on metallicity, it has an effect on the mass-loss rates ($\dot{M}$) of massive stars by $\dot{M} \propto Z^m$, where the index range of m is from 0.5 to 0.94 (Vink 2000; Vink et al. 2001; Mokiem et al. 2007). Rotation can enhance the mass-loss rate (Langer et al. 1998; Heger 1998). More importantly, rapid rotation can result in quasi-chemically homogeneous evolution (CHE) induced by various instabilities, such as dynamical shear

instability, Solberg-Hiøland instability, secular shear instability, Eddington-Sweet circulation and Goldreich Schubert-Fricke instability (e.g., Pinsonneault et al. 1989; Heger & Langer 2000). CHE can carry the heavy elements produced by nuclear burning in the core to the stellar surface, thus these heavy elements are able to enter the ISM via stellar wind (e.g., Brott et al. 2011; Song et al. 2016; Cui et al. 2018). The role of heavy element mixing is critical; it will affect the opacity of the envelope and increase the luminosity and effective temperature of the star (Glebbeek et al. 2009).

The standard non-rotating single-star model is strongly opposed as a possible progenitor of supernovae (SNe) (Fremling et al. 2014; Bersten & Nomoto 2014a), but Prantzos et al. (2018) recently reported the heavy element yields of rotating massive stars. They considered effects of three initial rotational velocities, namely, 0, 150 and 300 km s^{-1}. Initial velocity above ~ 350 km s^{-1} was more likely to attain the critical velocity (Meynet & Maeder 2006). Furthermore, in the VLT-FLAMES Tarantula Survey, Dufton et al. (2013) found that the projected rotational velocities of single early B-type stars can reach approximately 450 km s^{-1}. In binary systems, owing to mass transfer, rotation velocity will reach the Kepler velocity (de Mink et al. 2013).

Meanwhile, rapid rotation results in a more massive helium core via CHE (Belczynski et al. 2016; Eldridge & Maund 2016; Mandel & De Mink 2016; Marchant et al. 2016; Wang et al. 2018). On account of the helium-core, masses have strong effects on the remnant masses of neutron stars (NSs) and black holes (BHs) (e.g., Hurley et al. 2000; Belczynski et al. 2008). At the pre-supernova (pre-SN) stage, a larger helium-core burning produces a bigger CO-core (Meynet & Maeder 2006; Köhler et al. 2015; Marassi et al. 2019). Hence, rotation as well affects the heavy elements in CCSN ejecta. Very recently, in order to study dust formation in CCSN ejecta, Marassi et al. (2019) considered the effects of rotation, metallicity and fallback, in computing the heavy element yields of massive stars. However, they still did not consider the yields via stellar wind.

Therefore, it is necessary to study the heavy element yields coming from stellar wind and CCSN ejecta for massive stars. Even research on the relevant factors of elemental abundance is very urgent. In this paper, we study the effects of metallicity, rotation and fallback on the contribution of heavy elements produced by massive stars. In Section 2, the input physical parameters in models are described. The detailed results are discussed in Section 3. The main conclusions appear in Section 4.

2 MODEL

We use the open-source stellar evolution code Modules for Experiments in Stellar Astrophysics (MESA, version 10108, model CCSN) to simulate massive star evolutions (Paxton et al. 2011, 2013, 2015). In these simulations, we select a 67−isotope network. The mixing-length parameter ($\alpha_{\rm mlt}$) is taken as 1.5 (Brott et al. 2011; Moravveji 2016; Ma et al. 2020; Shi et al. 2020). In addition, the Ledoux criterion is connected with boundaries of convection, and semi-convection ($\alpha_{\rm sc}$) is selected as 0.02. Most of all, MESA has the Ledoux criterion $\nabla = \nabla_{\rm rad}$ in the overshoot area, which is different from the deep overshoot method (Maeder 1975; Viallet et al. 2015). Overshooting between the convective core and radiative one of the interior diffusion parameter is expressed by $f_{\rm ov} = 0.05$. Another effective parameter ($f_{\rm o} = 0.02$) is from the surface down to the overshoot layer (Paxton et al. 2011; Moravveji 2016; Higgins & Vink 2019). They are considered at all stages of evolution, and can also affect the total mass of stellar loss. Thermohaline mixing parameter ($\alpha_{\rm th}$) is equal to 2.0 (Kippenhahn et al. 1980; Paxton et al. 2013). In this work, we rely on the formulae of Vink et al. (2001) to calculate the mass-loss rates. In addition, rotation can enhance mass-loss rate by

$$\dot{M}(\Omega) = (\frac{1}{1-\Omega/\Omega_{\rm crit}})^{\gamma}\dot{M}(0), \qquad (1)$$

where $\dot{M}(0)$ is the mass−loss rate without rotation, Ω and $\Omega_{\rm crit}$ represent the angular velocity and critical Keplerian angular velocity, respectively, and parameter γ equals 0.43 (Langer et al. 1998). $\dot{M}(0)$ is calculated by the formulae in Vink et al. (2001). But when the angular velocity reaches the critical angular velocity, there will be a singularity. We limit the mass loss rate so that the mass loss time scale is longer than the thermal time scale of the star, see equations (1)–(3) in Yoon et al. (2012).

In order to discuss the effects of metallicity, the four initial metallicities are taken in different models as follows: [Fe/H]=0, [Fe/H]=–1, [Fe/H]=–2 and [Fe/H]=–3. Here, [Fe/H]=$\log[({\rm Fe/H})/({\rm Fe/H})_{\odot}]$ where [Fe/H]$_{\odot}$=0.02 is the solar metallicity (Thielemann et al. 2010; Chiaki et al. 2015).

Considering that rotational velocity of massive stars may get up to the critical velocity (de Mink et al. 2013) at the stellar surface, we take the initial rotational velocities in different simulations as 0, 300 and 500 km s^{-1}, respectively. Rotation triggers some instabilities, then leads to angular momentum transport and chemical mixing (e.g., Meynet 2012). Based on the research of Pinsonneault et al. (1989), Heger & Langer (2000) and Yoon & Langer (2006), MESA considers the ratio of turbulent viscosity to the diffusion coefficient ($f_{\rm c}$) and

the ratio of sensitivity to chemical gradients (f_μ) to calculate angular momentum transport and chemical mixing induced by rotation. Zhu et al. (2017) and Cui et al. (2018) employed MESA to investigate rotating massive stars. Following them, we choose f_c =0.0228 and f_μ =0.1, respectively.

MESA code can calculate the stellar evolution from pre-main sequence to CCSN. However, it cannot give the remnant masses after CCSN. In our work, following Hurley et al. (2000); Belczynski et al. (2008); Wang et al. (2018) the remnant masses of an NS or BH are given by the CO-core mass. When applying the CCSNe model of MESA via collapse of a core when the mass of Fe core $> 1.4\,M_\odot$, we do not consider nuclear reactions at this stage. The explosion mechanism of CCSNe is a complex process which still has not been explained well. In our model, the explosion energy (E) is 1×10^{51} erg (Nomoto et al. 2007; Paxton et al. 2013; Hirschi et al. 2017; Curtis et al. 2019).

Simultaneously, a supernova explosion occurs when stellar central density reaches 7.9×10^9 g cm^{-3} and central temperature is $\sim 6.5 \times 10^9$ K.

3 RESULTS

Using MESA code, we simulate the evolutions from main sequence (MS) to CCSN for eight massive stars with masses of 13, 15, 20, 25, 30, 40, 60 and 80 $M_\odot$. In order to discuss the effects of rotation, the initial rotational velocities are taken as 0, 300 and 500 km s^{-1} in different simulations. In order to check our model, we compare the evolutions of several stars with those in Brott et al. (2011) under similar input parameters. Figure 1 affirms that the evolutional tracks in two works are similar. All heavy elements originating from the star are produced by nucleosynthesis. They are ejected into the ISM via stellar wind and CCSN ejecta.

3.1 Heavy Elements Coming from Stellar Wind

Before massive stars trigger CCSNe, their heavy elements enter the ISM via stellar winds. These heavy elements are located in the stellar envelope. In this work, we estimate the yields of the i-th heavy element by

$$M_{\rm i} = \int_0^{t_{\rm pre}} \dot{M}(t) X_{\rm i}(t) {\rm d}t, \qquad (2)$$

where $t_{\rm pre}$ is the time from zero-age MS to pre-CCSN, and $\dot{M}(t)$ and $X_{\rm i}(t)$ are the mass-loss rate and the mass fraction of the i-th heavy element on the surface of the massive star, respectively. Therefore, the heavy elements coming from stellar wind mainly depend on the mass-loss rates and the chemical abundances on the stellar surface.

In our model, the mass-loss rates are affected by metallicity and rotational velocity. Figure 2 shows the evolutions of mass-loss rates for different initial mass stars with different metallicities and rotational velocities.

Comparing the two metallicity models, a high metallicity can result in a high mass-loss rate because $\dot{M} \propto Z^m$, where parameter m ranges from 0.64 to 0.85 (Vink et al. 2001). Simultaneously, as the mass-loss rates depend on the rotational velocities by Equation (1) mainly in the MS stage, we also consider the red supergiant (RSG) or Wolf-Rayet (WR) stage (Nugis & Lamers 2000). Therefore, the higher the initial rotational velocity is, the higher the mass-loss rate is. The mass-loss rate can be enhanced about 1–4 magnitudes when the initial rotational velocity increases from 0 to 500 km s^{-1}. The chemical abundances on stellar surfaces are determined by CHE. During MS late phase, the star begins to rapidly expand, and the rotational velocity sharply decreases. Therefore, CHE mainly works in MS phase. The heavy elements affected by nucleosynthesis during the MS phase are ^{12}C, ^{14}N and ^{16}O (key elements in the evolution of massive stars).

Figure 3 displays the evolutions of heavy-element (^{12}C, ^{14}N and ^{16}O) abundances on the stellar surfaces. Obviously, if there is no CHE in models without rotation, the heavy-element abundances on the stellar surface are constant during its life. However, in rotational models, the abundances of elements ^{12}C, ^{14}N and ^{16}O on the stellar surfaces change. ^{12}C and ^{16}O abundances decrease, while ^{14}N abundance increases. In particular, the lower the metallicity is, the stronger CHE is. Therefore, for lower metallicity models, the range of increase and decrease in abundance is more obvious. In addition, for the 60 $M_\odot$ panel, because the H-rich shell is stripped out before the RSG phase, the star enters the WR stage. As Figure 3 illustrates, elements ^{12}C and ^{16}O under the stellar surface strongly increase while the element ^{14}N decreases. Similar results have been discussed in Maeder & Meynet (2001), Hirschi et al. (2005), Chieffi & Limongi (2013), Groh et al. (2014) and Meyer et al. (2020).

Figure 4 depicts the yields of heavy elements (^{12}C, ^{14}N, ^{16}O and ^{56}Fe) produced via stellar winds. Hirschi et al. (2005b) also calculated the yields of heavy elements produced by stellar winds. In Table 3 for a model with $M_{\rm ini} = 20\,M_\odot$, [Fe/H] = 0 and $V = 300$ km s^{-1}, Hirschi et al. (2005b) reported the yields of elements ^{12}C, ^{14}N and ^{16}O to be $1.73 \times 10^{-2}, 4.30 \times 10^{-2}$ and $2.75 \times 10^{-2} M_\odot$, respectively. Under similar input parameters, the yields in our models are $3.34 \times 10^{-2}, 7.20 \times 10^{-2}$ and $4.32 \times 10^{-2}\,M_\odot$, respectively. For a model with $M_{\rm ini} = 40\,M_\odot$, the corresponding values in Hirschi et al. (2005b) are $1.60, 1.73 \times 10^{-1}$ and $3.34 \times 10^{-1}, M_\odot$, respectively, while in our work they are $1.15, 1.74 \times 10^{-1}$

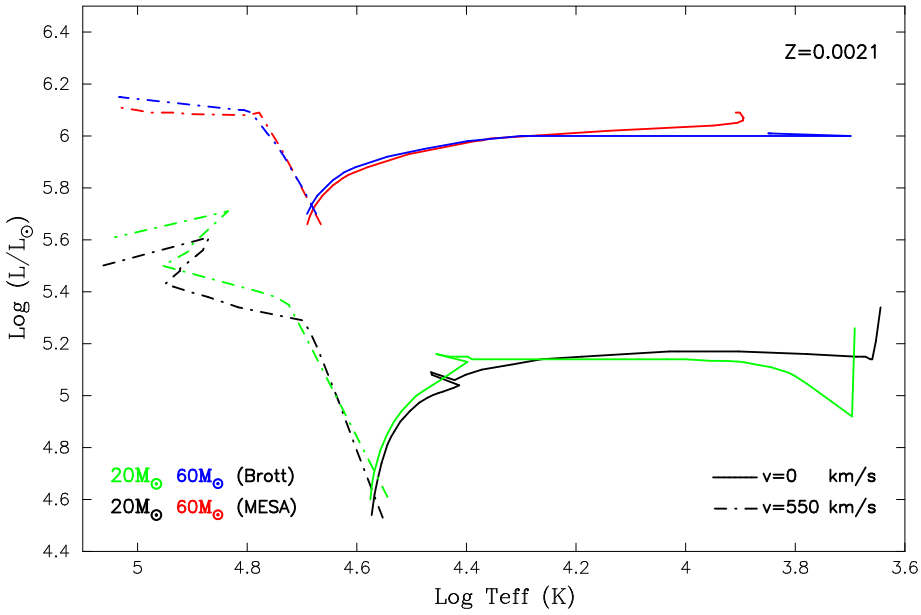

Fig. 1 The evolutions of massive stars with different masses and rotation velocities for $Z = 0.0021$. The *solid lines* represent a non-rotating star, while the *dash-dotted lines* signify a star with a rotation velocity of 550 km s^{-1}. *Green* and *blue lines* are the evolutional tracks calculated by Brott et al. (2011), and *black* and *red lines* are simulated in our models.

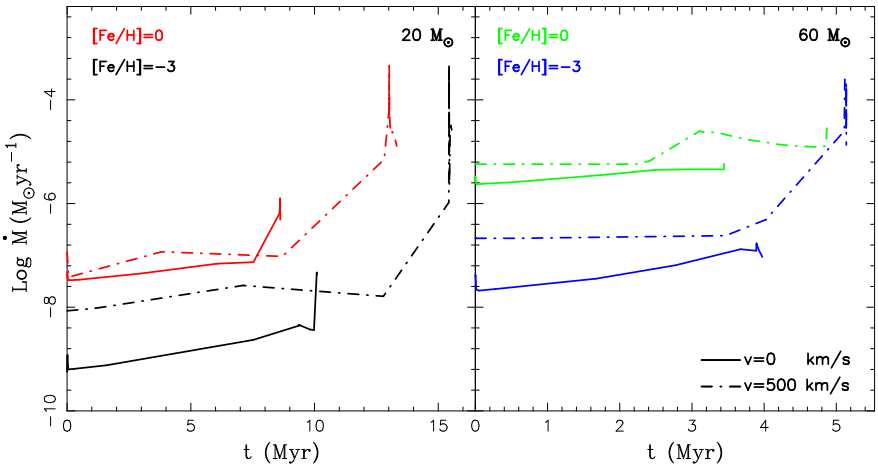

Fig. 2 The evolutions of mass-loss rates for models with different masses (20 and 60 $M_\odot$), metallicities ($[\mathrm{Fe/H}] = 0, -3$) and rotational velocities (0 and 500 km s^{-1}).

and $3.13 \times 10^{-1}\, M_\odot$, respectively. The results in both works are consistent.

In short, the yields of heavy elements coming from stellar winds can get to several $M_\odot$ for high rotation and high metallicity, but they may only be $10^{-2}\ M_\odot$ for low rotation and low metallicity.

3.2 Heavy Elements Coming from SN Ejecta

The heavy elements located in stellar interiors are ejected into the ISM via CCSN. They are mainly determined by mass fractions before CCSN occurs. Figures 5 and 6 feature the fractions of different elements in the models. For models with a mass of 20 $M_\odot$, rapid rotation can enhance mass-loss rates. A star with $V = 500$ km s^{-1} loses the whole hydrogen envelope. Simultaneously, it can trigger CHE, producing a larger CO-core. Therefore, compared with a star without rotation, it has a more massive core before CCSN. The stars with low metallicity can undergo efficient CHE and have low mass-loss rate. Their CO-cores at pre-CCSN are larger than those for stars with high metallicity. Similar results appear in models with a $60\,M_\odot$ star. These results are consistent with those in van Marle et al. (2007), Tominaga (2008) and Limongi & Chieffi (2018). During CCSN, massive stars eject a portion of their masses and leave compact objects (NSs or BHs). Generally, the remnant mass ($M_{\rm rem}$) is calculated by CO-core mass ($M_{\rm CO}$) (e.g., Belczynski et al.

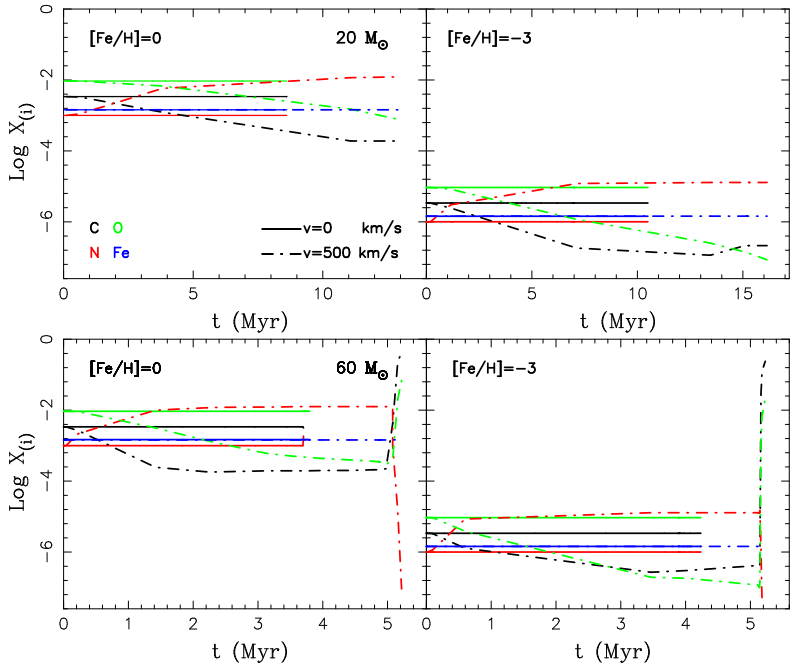

Fig. 3 The evolutions of heavy-element abundances [^{12}C (*black*), ^{14}N (*red*), ^{16}O (*green*) and ^{56}Fe (*blue*)] on the stellar surfaces for massive stars. The two panels in the top region represent the models with 20 $M_{\odot}$, while the two panels in the bottom region are for 60 $M_{\odot}$. The *solid* and *dash-dotted lines* represent models with $V = 0$ and 500 km s^{-1}, respectively. The different metallicities are given in the left-top region of every panel.

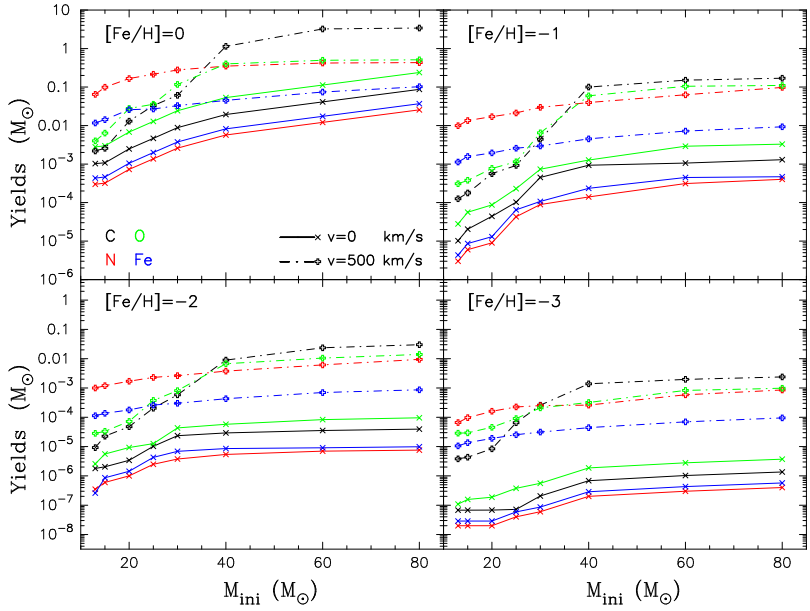

Fig. 4 The yields of the heavy elements, ^{12}C (*black*), ^{14}N (*red*), ^{16}O (*green*) and ^{56}Fe (*blue*), produced via stellar winds from massive stars with different initial masses, metallicities ([Fe/H] $= 0, -1, -2, -3$) and $V = 0$, 500 km s^{-1}. The multiplication and addition symbols represent calculated models with $V = 0$ and 500 km s^{-1}, respectively.

2008). In this work, we rely on equations (1) to (4) in Belczynski et al. (2008) to calculate $M_{\rm rem}$.

Figure 7(left) displays $M_{\rm CO}$ and $M_{\rm rem}$ calculated by different models. $M_{\rm CO}$ and $M_{\rm rem}$ are mainly determined by mass-loss rates. The stars with high metallicity and high rotational velocity have high mass-loss rates, and their $M_{\rm CO}$ and $M_{\rm rem}$ hardly exceed 10 $M_{\odot}$. CHE triggered by rapid rotation can only increase the $M_{\rm CO}$ and $M_{\rm rem}$ of models with initial masses lower than about 30 $M_{\odot}$. We compare the CO-core with the Belczynski et al. (2008) model with a rotation of 300 km s^{-1}; obviously the sizes of the CO-cores in the two models are consistent.

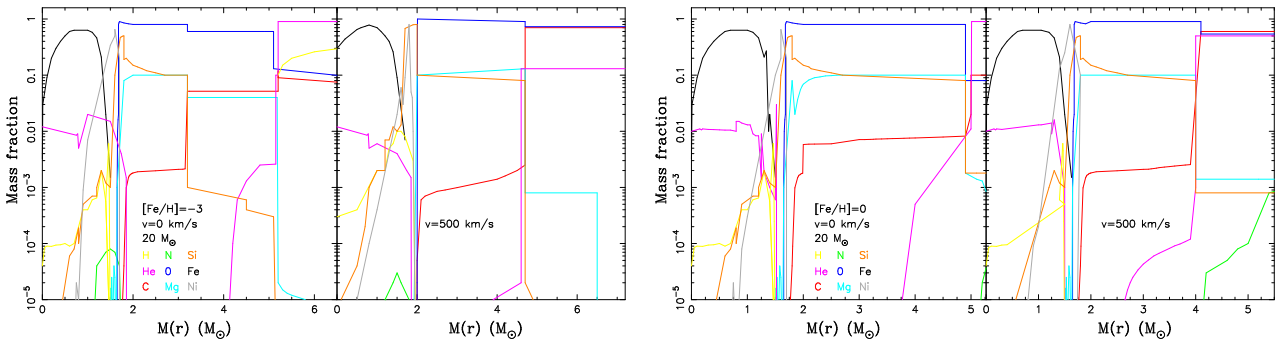

Fig. 5 The mass fractions of chemical elements in stellar interiors $[M(r)]$ at pre-CCSN for models with initial mass of 20 $M_\odot$. The left two panels (the initial rotational velocities are 0 and 500 km s^{-1} in the *left* and *right* subpanels respectively) represent the models with $[\mathrm{Fe/H}] = -3$, and the right two panels are for models with $[\mathrm{Fe/H}] = 0$. The abundance of various chemical elements is represented by colored lines, for example, ^{1}H (*yellow*), ^{12}C (*red*), ^{14}N (*green*), etc.

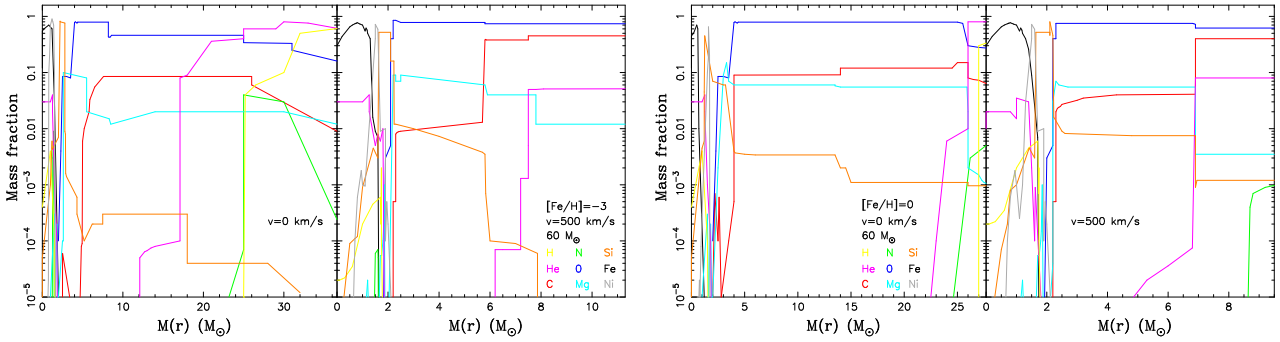

Fig. 6 Similar to Fig. 5 but for models with initial mass of 60 $M_\odot$.

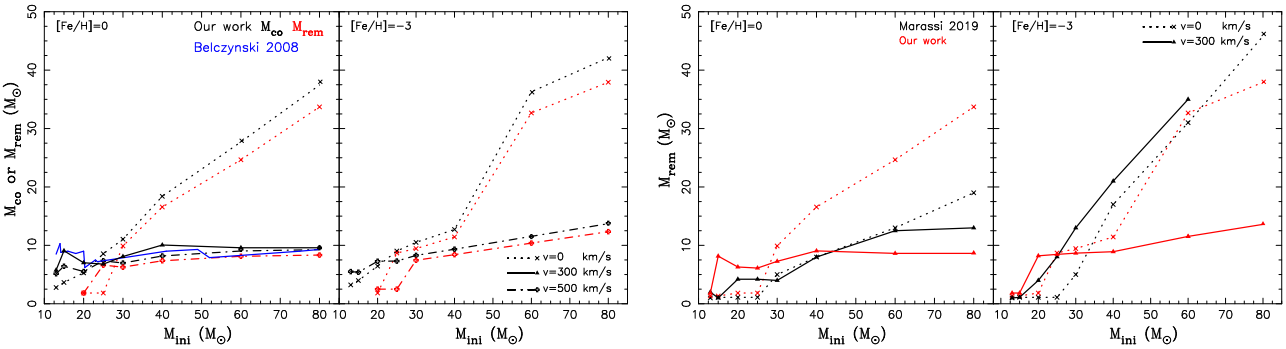

Fig. 7 *Left*: the CO-core ($M_{\rm CO}$) and remnant ($M_{\rm rem}$) masses vs. the initial masses in different models. The *black* and *red lines* represent $M_{\rm CO}$ and $M_{\rm rem}$, respectively (Our work). The *solid blue line* signifies the CO-core size of the Belczynski et al. (2008) model with a rotation of 300 km s^{-1}. *Right*: comparison of the remnant masses in our work with those in Marassi et al. (2019). *Black* and *red lines* correspond to results from Marassi et al. (2019) and our work respectively.

Figure 7(right) compares $M_{\rm rem}$ calculated by this work with those in Marassi et al. (2019). Obviously, $M_{\rm rem}$ of stars with initial masses lower than about 30 $M_\odot$ in our work is higher than that in Marassi et al. (2019), while others in our work are lower. The main reasons are mass-loss rates and the method for calculating remnant mass. For the former, as figure 2 in Marassi et al. (2019) demonstrates, the hydrogen envelope with a mass of about 3 $M_\odot$ in the model with initial mass 60 $M_\odot$ and [Fe/H]=–1 is left before CCSN. However, under the model with [Fe/H]=–1, there is no hydrogen envelope for intial mass 60 $M_\odot$ at pre-CCSN. For the latter, the remnant mass in Marassi et al. (2019) is determined by the initial mass and metallicity, while this work calculates $M_{\rm rem}$ via $M_{\rm CO}$. Observation affirms that the CO nucleus will only appear when the gas density of the star reaches the standard value (Chen et al. 2006). The yield of the i-th element produced by CCSN ejecta can be calculated by explosion.

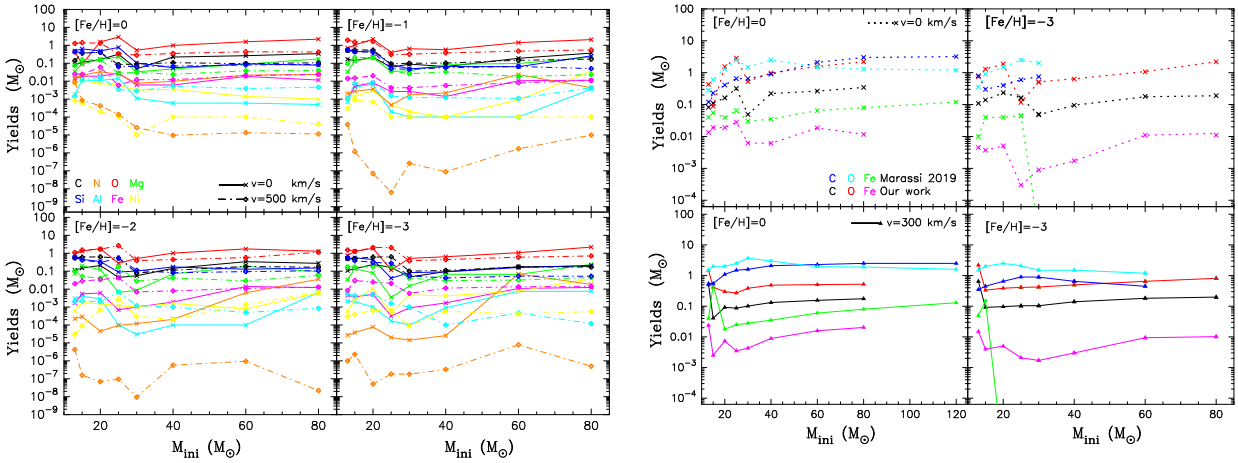

Fig. 8 Yields of heavy elements produced by CCSN ejecta. The *left* panel represents the results in this work. The *right* panel gives a comparison of our results with ones in Marassi et al. (2019).

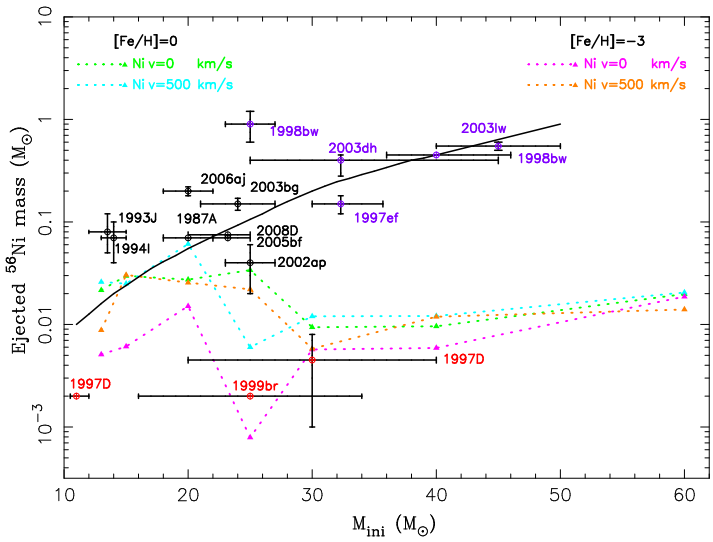

Fig. 9 The ^{56}Ni masses produced by CCSN ejecta and their progenitor masses at MS phase. These data come from Nomoto et al. (2013). The *red*, *black* and *purple cycles* represent faint SNe, normal SNe and hypernovae, respectively. The yields of ^{56}Ni calculated by our models are signified by *dotted lines* ($[\mathrm{Fe/H}] = 0$) and *dashed lines* ($[\mathrm{Fe/H} = -3$). For example, the *green* and *blue colors* represent models with $V = 0$ and 500 km s^{-1}, respectively.

Figure 8 shows the yields of heavy elements produced by CCSN ejecta in this work.

$$M_{\mathrm{i}} = \int_{\mathrm{M_{rem}}}^{M_{\mathrm{fin}}} [X_{\mathrm{i}}(m) - X_{\mathrm{i}}^{0}]\mathrm{d}m\,, \tag{3}$$

where $X_{\mathrm{i}}(m)$ is the i-th element mass fraction before the SN with Lagrangian coordinate m and X_{i}^{0} is the initial abundance; the X_{i}^{0} values of these elements are 0. M_{fin} is the final mass of the star (Ekström et al. 2008). However, compared with stellar winds (see Fig. 4), CCSN ejecta can produce more heavy elements, especially elements heavier than ^{16}O. Compared with Marassi et al. (2019), our work gives lower yields of heavy elements. The main reason is that our models have higher mass-loss rates. Before CCSN occurs, the stars in our models have lost more mass than those in Marassi et al. (2019).

Via the comparison of observed light curves and theoretical models, Nomoto et al. (2013) estimated the ^{56}Ni masses produced by some CCSN ejecta and their progenitor masses, which are featured in Figure 9. Here, ^{56}Ni is caused by the decay of ^{56}Ni $\rightarrow$ ^{56}Co $\rightarrow$ ^{56}Fe (Argast et al. 2002; Hamuy 2003). We calculate the yields of ^{56}Ni in the different initial mass models. Similar to the fixed energy models in Marassi et al. (2019), our results only explain the ^{56}Ni masses produced by faint SNe or normal SNe with progenitor masses lower than 25 $M_{\odot}$. Clearly, our understanding of massive star evolution and the process involved in a CCSN is still poor.

4 CONCLUSIONS

In this work, we calculate the contribution of heavy elements from massive stars via stellar wind and CCSN ejecta to ISM.

In our models, the evolutions of massive stars are affected by rotation, mass-loss rate and metallicity. The rotation via CHE changes the chemical abundances of stellar surfaces, and enhances mass-loss rate. It can increase ^{14}N abundance by 10 times while decreasing ^{12}C and ^{16}O abundances by similar amounts. It can enhance the mass-loss rates by about 1–4 magnitude when the initial rotational velocity increases from 0 to 500 km s^{-1}. Therefore, the yields of heavy elements coming from stellar winds are mainly affected by stellar rotation. We estimate that the stellar wind can produce heavy element yields of about 10^{-2} (for low metallicity models) to a mass of several $M_{\odot}$ (for low metallicity and rapid rotation models), which depends on stellar rotation and metallicity.

The yields of heavy elements produced by CCSN ejecta depend not only on rotation, mass-loss rate and metallicity, but also on the remnant mass of massive stars. Here, the latter mainly depends on the mass of the CO-core which is greatly affected by the above three parameters. Our models calculate that the yields of heavy elements produced by CCSN ejecta can reach a mass of up to several $M_{\odot}$. Compared with stellar wind, CCSN ejecta has a greater contribution to the heavy elements in ISM.

We also compare the ^{56}Ni yields calculated in this work with observational estimates. Our models only explain the ^{56}Ni masses produced by faint SNe or normal SNe with progenitor masses lower than about 25 $M_{\odot}$, and greatly underestimate the ^{56}Ni masses produced by stars with initial masses higher than about 30 $M_{\odot}$. It means that there is still a long way go in understanding massive star and CCSN evolution.

Acknowledgements This work received generous support from the National Natural Science Foundation of China (Grant Nos. 11763007, 11863005, 11803026 and U2031204). We would also like to express our gratitude to the Natural Science Foundation of Xinjiang (No. 2021D01C075) and the Tianshan Youth Project of Xinjiang (No. 2017Q014).

References

Ablimit, I., & Maeda, K. 2018, ApJ, 866, 151
Argast, D., Samland, M., Thielemann, F. K., & Gerhard, O. E. 2002, A&A, 388, 842
Belczynski, K., Kalogera, V., Rasio, F. A., et al. 2008, ApJS, 174, 223
Belczynski, K., Heger, A., Gladysz, W., et al. 2016, A&A, 594, A97
Bersten, M., & Nomoto, K. 2014a, in Binary Systems, their Evolution and Environments, 36
Brott, I., Evans, C. J., Hunter, I., et al. 2011, A&A, 530, A116
Castor, J., McCray, R., & Weaver, R. 1975, ApJL, 200, L107
Chen, X., Xu, Y., Shen, Z., & Li, J. 2006, Science in China Series G: Physics, Mechanics and Astronomy, 49, 1862
Chiaki, G., Marassi, S., Nozawa, T., et al. 2015, MNRAS, 446, 2659
Chieffi, A., & Limongi, M. 2004, VizieR Online Data Catalog, J/ApJ/608/405
Chieffi, A., & Limongi, M. 2013, ApJ, 764, 21
Cui, Z., Wang, Z., Zhu, C., et al. 2018, PASP, 130, 084202
Curtis, S., Ebinger, K., Fröhlich, C., et al. 2019, ApJ, 870, 2
de Mink, S. E., Langer, N., Izzard, R. G., Sana, H., & de Koter, A. 2013, ApJ, 764, 166
Du, F. 2020, arXiv e-prints, arXiv:2007.11294
Dufton, P. L., Langer, N., Dunstall, P. R., et al. 2013, A&A, 550, A109
Dunne, L., Eales, S., Ivison, R., Morgan, H., & Edmunds, M. 2003, Nature, 424, 285
Duolikun, A., Zhu, C., Wang, Z., et al. 2019, PASP, 131, 124202
Ekström, S., Meynet, G., Chiappini, C., Hirschi, R., & Maeder, A. 2008, A&A, 489, 685
Eldridge, J. J., & Maund, J. R. 2016, MNRAS, 461, L117
Fremling, C., Sollerman, J., Taddia, F., et al. 2014, A&A, 565, A114
Glebbeek, E., Gaburov, E., de Mink, S. E., Pols, O. R., & Portegies Zwart, S. F. 2009, A&A, 497, 255
Groenewegen, M., & de Jong, T. 1993, in European Southern Observatory Conference and Workshop Proceedings, 46, 101
Groh, J. H., Meynet, G., & Ekström, Sylvia andGeorgy, C. 2014, A&A, 564, A30
Guo, Y., Liu, D., Wu, C., & Wang, B. 2020, arXiv e-prints, arXiv:2008.00866
Hamuy, M. 2003, IAU Circ., 8146, 3
Heger, A. 1998, The Presupernova Evolution of Rotating Massive Stars, Garching, Germany: Max-Planck-Institut Fur Astrophysik, QB1000, H433
Heger, A., & Langer, N. 2000, ApJ, 544, 1016
Heger, A., & Woosley, S. E. 2010, ApJ, 724, 341
Higgins, E. R., & Vink, J. S. 2019, A&A, 622, A50
Hirschi, R., Arnett, D., Cristini, A., et al. 2017, in IAU Symposium, 331, Supernova 1987A: 30 Years Later - Cosmic Rays and Nuclei from Supernovae and Their Aftermaths, eds. A. Marcowith, M. Renaud, G. Dubner, A. Ray, & A. Bykov, 1
Hirschi, R., Meynet, G., & Maeder, A. 2005, Nucl. Phys. A, 758, 234
Hirschi, R., Meynet, G., & Maeder, A. 2005b, A&A, 433, 1013
Hix, W. R. 2001, Nuclear Reaction Rate Uncertainties and Their Effects on Nova Nucleosynthesis Modeling, arXiv: 08133, Tech. rep.
Hurley, J. R., Pols, O. R., & Tout, C. A. 2000, MNRAS, 315, 543
José, J., Hernanz, M., & Iliadis, C. 2006, Nucl. Phys. A, 777, 550

Kippenhahn, R., Ruschenplatt, G., & Thomas, H. C. 1980, A&A, 91, 181
Köhler, K., Langer, N., de Koter, A., et al. 2015, A&A, 573, A71
Langer, N., Heger, A., & García-Segura, G. 1998, Reviews in Modern Astronomy, 11, 57
Li, F., Zhu, C., Lü, G., & Wang, Z. 2016, PASJ, 68, 39
Limongi, M., & Chieffi, A. 2018, ApJS, 237, 13
Lü, G., Zhu, C., & Podsiadlowski, P. 2013, ApJ, 768, 193
Ma, Y.-C., Liu, H.-L., Zhu, C.-H., et al. 2020, RAA (Research in Astronomy and Astrophysics), 20, 049
Maeder, A. 1975, A&A, 43, 61
Maeder, A., & Meynet, G. 2001, A&A, 373, 555
Maeder, A., & Meynet, G. 2012, Reviews of Modern Physics, 84, 25
Mandel, I., & De Mink, S. 2016, in 41st COSPAR Scientific Assembly, Vol. 41, E1.16
Marassi, S., Schneider, R., Limongi, M., et al. 2019, MNRAS, 484, 2587
Marchant, P., Langer, N., Podsiadlowski, P., Tauris, T. M., & Moriya, T. J. 2016, A&A, 588, A50
Marigo, P. 2007, in Astronomical Society of the Pacific Conference Series, 378, Why Galaxies Care About AGB Stars: Their Importance as Actors and Probes, eds. F. Kerschbaum, C. Charbonnel, & R. F. Wing, 392
Meyer, D. M. A., Petrov, M., & Pohl, M. 2020, MNRAS, 493, 3548
Meynet, G. 2000, in IAU Joint Discussion, 24, 11
Meynet, G. 2012, in Chemical Evolution of the Milky Way, 20
Meynet, G., & Maeder, A. 2006, Single Massive Stars at the Critical Rotational Velocity, Astronomical Society of the Pacific Conference Series, 355, 27
Mokiem, M. R., de Koter, A., Vink, J. S., et al. 2007, A&A, 473, 603
Moravveji, E. 2016, MNRAS, 455, L67
Nomoto, K., Kobayashi, C., & Tominaga, N. 2013, Annual Review of Astronomy and Astrophysics, 51, 457
Nomoto, K., Tominaga, N., Tanaka, M., Maeda, K., & Umeda, H. 2007, in American Institute of Physics Conference Series, 937, Supernova 1987A: 20 Years After: Supernovae and Gamma-Ray Bursters, eds. S. Immler, K. Weiler, & R. McCray, 412
Nomoto, K., Tominaga, N., Umeda, H., Kobayashi, C., & Maeda, K. 2006, Nucl. Phys. A, 777, 424
Nugis, T., & Lamers, H. J. G. L. M. 2000, A&A, 360, 227
Paxton, B., Bildsten, L., Dotter, A., et al. 2011, ApJS, 192, 3
Paxton, B., Cantiello, M., Arras, P., et al. 2013, ApJS, 208, 4
Paxton, B., Marchant, P., Schwab, J., et al. 2015, ApJS, 220, 15
Pinsonneault, M. H., Kawaler, S. D., Sofia, S., & Demarque, P. 1989, ApJ, 338, 424
Prantzos, N., Abia, C., Limongi, M., Chieffi, A., & Cristallo, S. 2018, MNRAS, 476, 3432
Puls, J., Vink, J. S., & Najarro, F. 2008, A&A Rev., 16, 209
Rukeya, R., Lü, G., Wang, Z., & Zhu, C. 2017, PASP, 129, 074201
Shi, Y., Xue, X., Zhu, C., et al. 2020, RAA, v.20, 37
Smith, N. 2014, Constraining the Mass in Cool Dust Shells Around Massive Stars
Song, H. F., Meynet, G., Maeder, A., Ekström, S., & Eggenberger, P. 2016, A&A, 585, A120
Thielemann, F. K., Dillmann, I., Farouqi, K., et al. 2010, in Journal of Physics Conference Series, Vol. 202, 012006
Tominaga. 2008, The Astrophysical Journal, 690, 526
van Marle, A. J., Langer, N., Achterberg, A., & García-Segura, G. 2007, 30, 1
Viallet, M., Meakin, C., Prat, V., & Arnett, D. 2015, A&A, 580, A61
Vink, J. S. 2000, Radiation-driven Wind Models of Massive Stars, PhD thesis, Universiteit Utrecht
Vink, J. S., de Koter, A., & Lamers, H. J. G. L. M. 2001, A&A, 369, 574
Wang, T., Li, L., Zhu, C., et al. 2018, ApJ, 863, 17
Woosley, S. E., & Weaver, T. A. 1995, ApJS, 101, 181
Yoon, S. C., Dierks, A., & Langer, N. 2012, A&A, 542, A113
Yoon, S. C., & Langer, N. 2006, in Astronomical Society of the Pacific Conference Series, 353, Stellar Evolution at Low Metallicity: Mass Loss, Explosions, Cosmology, eds. H. J. G. L. M. Lamers, N. Langer, T. Nugis, & K. Annuk, 63
Zhu, C., Liu, H., Lü, G., Wang, Z., & Li, L. 2019, MNRAS, 488, 525
Zhu, C., Lü, G., & Wang, Z. 2017, ApJ, 835, 249
Zhu, C., Lü, G., Wang, Z., & Liu, J. 2013, PASP, 125, 25